Effects of Debonding and Fiber Strength Distribution on Fatigue-Damage Propagation in Carbon Fiber-Reinforced Epoxy

E. K. GAMSTEDT

Materials Research Department, Risø National Laboratory, P.O. Box 49, DK-4000 Roskilde, Denmark

Received 24 February 1999; accepted 20 August 1999

ABSTRACT: In order to design new fatigue-resistant composites, the underlying fatigue damage mechanisms must be characterized and the controlling microstructural properties should be identified. The fatigue-damage mechanisms of a unidirectional carbon fiber–reinforced epoxy has been studied under tension–tension loading. A ubiquitous form of damage was one or a few planar fiber breaks from which debonds or shear yield zones grew in the longitudinal direction during fatigue cycling. This leads to a change in stress profile of the neighboring fibers, and an increase in failure probability of these fibers. The breakage of fibers in the composite is controlled by the fiber strength distribution. The interaction between the fiber strength distribution and debond propagation leading to further fiber breakage was investigated by a numerical simulation. It was found that a wider distribution of fiber strength and a higher debond rate lead to more distributed damage and a higher fracture toughness. Implications to fatigue life behavior are discussed, with reference to constituent microstructure. © 2000 John Wiley & Sons, Inc. J Appl Polym Sci 76: 457–474, 2000

Key words: fatigue; mechanisms; carbon fiber/epoxy; debonding; fiber breakage

INTRODUCTION

Polymer matrix composites have gained increased use in load carrying applications during the last few decades. The most frequent failure mode for structural materials is fatigue.[1] If the fatigue mechanisms were known together with the controlling microstructural parameters (e.g., shear yield stress of the polymer matrix, fiber-matrix interfacial fracture toughness, fiber strength), more fatigue-resistant materials could be designed, which would lead to lighter and more slender composite structures. For instance, the polymer could be synthesized in a way that would increase its crack-growth resistance, which in turn would suppress or inhibit fatigue degradation and eventual failure.

Composite failure, both under static and fatigue conditions, is intrinsically localized, i.e., failure occurs in the weakest volume element. In this element, the microstructure is generally in the same size scale as the failure inducing damage. Individual fiber breaks, debonds, bridged cracks, yielded matrix zones, etc. may have to be considered. Since lifetime prediction is an ultimate goal in the extension of studies of fatigue mechanisms, failure and localized damage have to be considered. This means that it is necessary to take the heterogeneous microstructure of the composite into account in the analysis of fatigue-damage growth.

Simple damage scenarios that have been experimentally identified should be the first to be modeled, which typically involve single damage sites. Next, this can be extended to more complex

Correspondence to: E. K. Gamstedt (kristofer.gamstedt@risoe.dk).

Journal of Applied Polymer Science, Vol. 76, 457–474 (2000)

situations with, e.g., cluster formation and coalescence, and volume scaling. One of the potential benefits of microscopic modeling of fatigue degradation is that judicious parametric studies can indicate improvements in the constituent properties for microstructural tailoring and optimum macroscopic performance when experiments are not feasible.

For structural applications of composite materials, laminates containing unidirectional plies are preferably used. The layup of the laminate can be tailored to suit the applied stress state. An almost ubiquitous ply has its fibers aligned in the longitudinal direction (0°), i.e., in the direction of the largest principal stress. In fatigue of multidirectional laminates, the 0° ply controls the fatigue life of the entire laminate when interpreted in terms of applied initial strain.[2–4] This is because the 0° plies have the largest strain to failure, and have longer fatigue lives than plies with oblique reinforcement for a given strain amplitude.[5,6] Also, damage in off-axis plies seems to have little influence on the stress state in the 0° plies.[7] Because of the relative importance of the 0° ply in fatigue of composite laminates, only this ply will be investigated here.

There are two main approaches to model damage accumulation in unidirectional 0° composites through the successive breakage of individual fibers, depending on how the load is redistributed among the surviving fiber segments when a fiber is broken. These are called (1) global load sharing and (2) local load sharing. In composites with weak interfaces, the global load-sharing concept can be used. It assumes that all remaining intact fibers share the load equally in the plane of the fiber breaks. This is locally analogous to a loose fiber bundle with no stress transfer between contiguous fibers. For polymer-matrix composites, this is generally a poor presumption, since the interfacial adhesion is usually fairly efficient, and the relatively high stress-transfer ability results in localized damage with small critical flaws at the initiation of catastrophic failure. Instead, local load sharing can be adopted, in which only the neighboring fibers to a fiber break are assumed to share the additional load according to an empirical or physical stress redistribution function. The local load-sharing scheme becomes more detailed, and generally mathematically more intricate, but forms a more physical description that is more consistent with experimental data. The local load-sharing approach will implicitly be advocated for the debond model in the present study. A well-reasoned and versatile semianalytical local load-sharing model based on the shear-lag principle developed by Beyerlein and Phoenix[8] will be used here.

In this work, the active fatigue damage mechanisms have been identified in a commercial 0° carbon fiber–reinforced epoxy by a surface-replication technique. Based on these findings, a parametric investigation was undertaken, where the influence of the interaction of the observed damage modes on fatigue-damage accumulation was studied.

EXPERIMENTAL

Unidirectional carbon fiber/epoxy specimens were fabricated with a $[0_4]_T$ stacking sequence of AS4/8552 prepreg plies from Hexcel. The matrix is a thermoplastic-modified epoxy system. The prepreg material was autoclave-cured according to the manufacturer's recommendations at 180°C and 6 bar for 120 min. During the autoclave process, a well-polished plate of stainless steel was placed inside the vacuum bag directly on top of the release film covering the stacked prepreg plies, to enhance the surface smoothness and to prevent the usual texture on the upper surface of the composite from the release fabric or surface bleeder. As a result, more excess resin was bled than for a conventional cure process without a pressure plate, and a fiber volume fraction of $\sim$ 63% was obtained. The specimens were cut with an abrasive water jet to dimensions recommended by ASTM standard D3039: a 127-mm gage length and a 12.7-mm width. Tapered end tabs of glass weave–reinforced epoxy were bonded to the laminates by an adhesive epoxy film cured at 125°C for 2 h. The specimen edges were subsequently polished with successively finer silicon carbide papers ending with 2400 grit. This conveyed edges with a glossy and scratch-free appearance.

The specimens were subjected to load-controlled fatigue tests on an Instron 1272 machine. The longitudinal strains were registered on a personal computer with a Sandner A10-2.5 extensometer with a gage length of 10 mm. The closed-loop fatigue tests consisted of a sinusoidal load with a frequency of 10 Hz. The stress ratio was continually $R = 0.1$. All tests were performed at room temperature.

During the course of the fatigue, a sequence of surface replicas were intermittently taken at the

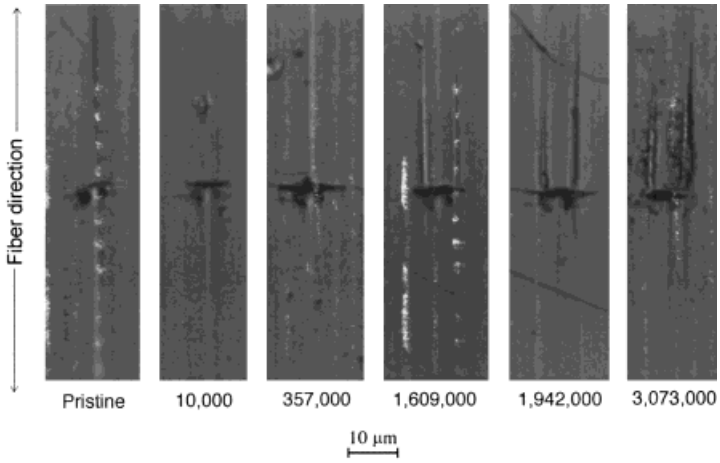

Figure 1 Growth of debonds from a single fiber break (fiber diameter ~ 5 μm).

same position in the middle of a specimen surface. Since longitudinal splitting tends to occur at the edges of unidirectional coupons due principally to fiber misalignment, the replicas were taken on the unpolished surface across the width. A cellulose acetate film was plasticized with an acetone-based solution and thereafter pressed onto a predesignated position on the specimen surface for 2 min. As the solution evaporated, the polymer film was allowed to harden. Before each replication, the surface spot was carefully cleaned with ethanol and dried. The peak load was applied to the specimen during the replication to allow the cracks to open and render them more visible. The replicas were taken to a maximum strain of 0.89%, which is close to the fatigue limit of this material. After replication, a carbon coating with a thickness of 30 to 50 nm was sputtered on the replica samples to improve the image resolution in the optical and scanning electron microscopes. The development of fatigue damage was mapped by locating a large damage site on the replica with the highest number of elapsed cycles, and relocating the same site on the previous replicas from the same set with a lower number of cycles. Since the damage sites were dispersed and rare, a map with reference points such as scratches, misaligned fibers, etc. had to be drawn to relocate the position of the fatigue damage.

Scanning electron micrographs were taken on carbon-coated replica films in a JEOL JSM-T300 scanning electron microscope with an accelerating voltage of 20 kV. The replicas were also examined by optical microscopy with a built-in microscope of a Matzusawa MXT-α microhardness tester.

EXPERIMENTAL RESULTS AND DISCUSSION

The macroscopic fatigue-life behavior (in terms of fatigue-life curves) for the carbon fiber/epoxy material is reported elsewhere.[9] It showed fatigue degradation with a sloping fatigue life curve. In contrast, earlier carbon fiber/epoxy materials with very high modulus fibers did not show progressive damage, and hence a horizontal fatigue-life scatter band located at the static fiber strain to failure.[10] The fatigue sensitivity of the present material must be due to a set of progressive fatigue-damage mechanisms, which give rise to damage propagation and eventual failure.

The surface replicas showed that the most frequent type of progressive fatigue-damage mechanisms was isolated single or multiple fiber breaks from which debonds grew with an increasing number of elapsed load cycles. Figure 1 presents a sequence of replicas of a single fiber break with growing debonds. In Figure 2, the debond lengths are plotted with respect to the number of load cycles.

Since the fibers have a distribution in strength, or in strain to failure, some of them will break even at low applied strains well below the average value of the strain to failure. When a fiber surrounded by intact fibers has been broken, shear stresses are induced that can be relaxed by interfacial debonding, propagation of matrix cracks, or shear yield zones along the interface. All of these progressive mechanisms result in a stress relaxation of the polymer matrix next to the fiber break, and a continuous change in the stress profile of the intact neighboring fibers. Only debonding will be considered in the model because of the

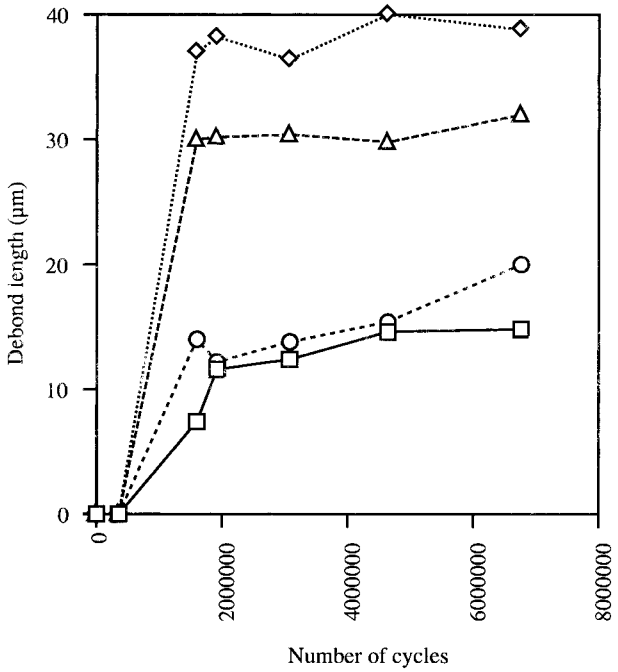

Figure 2 Debond propagation from a single fiber break (accuracy ~ 2 μm).

apparent similarity between the effects of the different mechanisms, and the fact that debonding was the most prevalent progressive mechanism. In Figure 3, an example is shown where a shear yield zones grew from one end of the plane of multiple fiber breaks, whereas debonds emanated from the other end. A third example with debonds propagating from a site of multiple fiber break is presented in Figure 4. However, the most prevalent form of observed fatigue damage was only one fiber break from which debonds propagated. A cluster of planar multiple fiber breaks has essentially the same effect on the neighboring fibers as a single fiber break; only the stress concentration[11] and the shear stresses[12] are larger.

Despite that the direction of the applied load is parallel to the fibers, the cracks (i.e., debonds) do not grow perpendicular to this direction, which is customary to monolithic isotropic materials. The degree of material anisotropy is very high for unidirectional 0° composites. For example, the transverse strength is significantly lower than the tensile strength. This anisotropy leads to longitudinal growth of cracks in mode II along the fiber–matrix interface due to low interfacial strength and the large mismatch in elastic properties. This trend prevails for short-fiber composites also. Friedrich et al.[13] tested injection-molded short-fiber composites in fatigue, and noticed crack propagation in the principal material direction independent of the load direction. Xian and Choy[14] tested notched carbon fiber/bismaleimide in fatigue, and observed mode II propagation in the fiber direction for 0° specimens. In composites with long continuous fibers in the load direction, debonds may initiate from the distributed fiber breaks and propagate under fatigue. As mentioned previously, the growing debond continuously changes the local load of the neighboring fibers. When a weak element of an intact fiber is overloaded, it may fail and give rise to new debonds, etc. In this manner, fiber breaks will be accumulated, and the material will eventually fail, as schematically depicted in Figure 5. This scenario can also be combined with cycle- or time-dependent growth of a yield or creep zone in front of the interfacial debond.[15] Due to the growth of debonds and yield zones, the final fatigue crack will have a nonplanar fracture surface. Depending on the direction of matrix crack growth, different patterns of damage growth occur. If the matrix crack grows perpendicular to the load and fiber direction, a fiber-bridged crack may form.[9] As discussed later, if the material is prone to debonding in the longitudinal direction, there will be nonplanar successive fiber breakage. There is substantial experimental evidence in polymer-matrix composites of debonding in fatigue.[16–19]

The evolution of stress transfer during fatigue debond growth and the resulting successive breakage of fibers are key mechanisms in polymer-matrix composites that are prone to debonding. In order to model this behavior and ultimately predict fatigue life, the fundamental and basic configurations must first be investigated and understood. A simple case with one fiber break from which uniform debonds grow along the fiber will be investigated parametrically to shed some light on the interaction between stochastic fiber breakage and debond propagation. From the results, some qualitative conclusions on macroscopic fatigue behavior can be drawn.

In fatigue, the progression of any damage, debonding subsumed, should be described by a kinetic equation to predict the rate of damage development. Combined with a failure criterion, predictions of fatigue life would be possible. A kinetic relationship for debond growth can and should be measured experimentally. The growth rates from the replica measurements of the type presented in Figure 2 is relevant only to itself, as the stress state and interfacial toughness vary

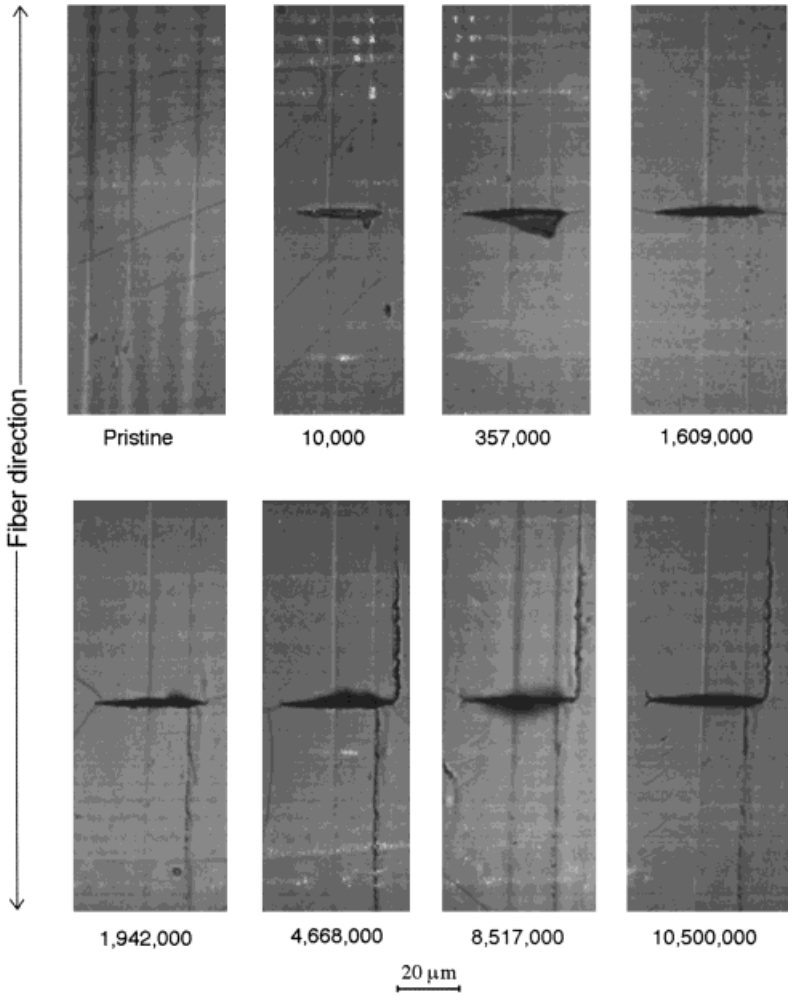

Figure 3 Growth of shear yield zones (left) and debonds (right) from a set of plane fiber breaks (fiber diameter $\sim$ 5 μm).

from fiber to fiber, and along each fiber. The growing debonds showed an irregular accelerating–decelerating growth pattern, which could be explained by a variability in interface properties along the fibers. This behavior would require a stochastic growth model. Furthermore, these measurements were made on the surface of a composite with a disordered microstructure, which means that data reduction to a generic growth law is not straightforward. No kinetic law for the debond propagation will be considered here, since the conceived model is not a direct description of experimental results, but rather aims for a parametric study to assess influences of debonding and fiber strength variability on fiber breakage under fatigue conditions. However, for future attempts to life predictions a kinetic law is an exigency.

Since the advent of micro-Raman spectroscopy, the composite research community has been endowed with a powerful tool to study local stresses and strains in composites reinforced by fibers with crystalline or turbostratic morphologies. Ideally, micro-Raman spectroscopy could be used to investigate in detail the influence of the microstructural properties (e.g., debond growth law and fiber strength distribution) on damage accumulation and failure in composites exhibiting the observed fatigue micromechanisms. Since these properties cannot be controlled independently of other properties, and experiments would be too costly, we turn toward numerical simulation. A two-dimensional shear-lag approach will be used to model the composite stress state. It is best to first gain understanding of the micromechanical interactions of fiber ruptures and debond propa-

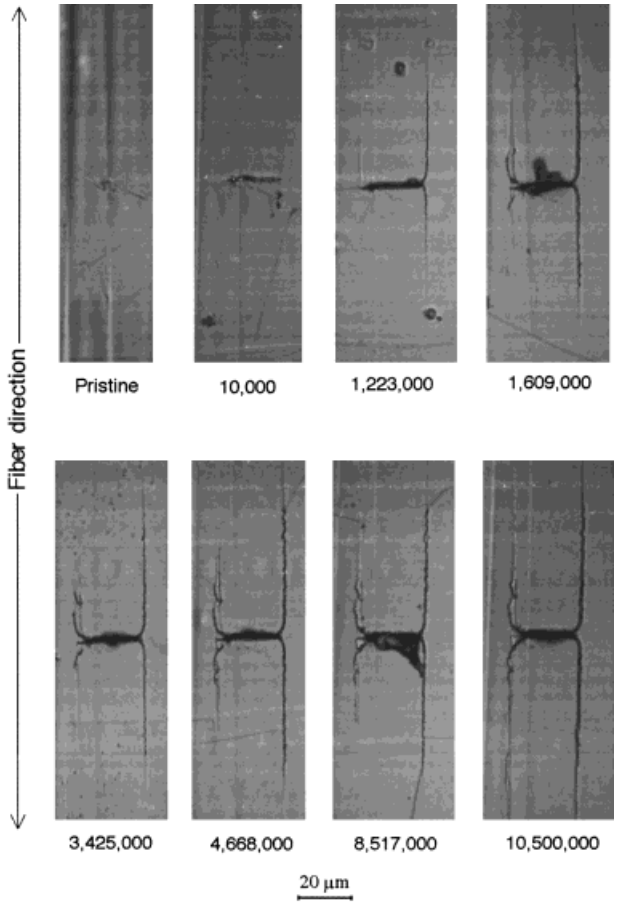

Figure 4 Growth of debonds from a set of plane fiber breaks (fiber diameter ~ 5 μm).

gation in two dimensions before extending the analysis to three dimensions. Furthermore, early experimental work has shown similar failure behavior in single monolayers and in composites composed of stacked multiple layers.[21,22]

NUMERICAL SIMULATION

Shear-Lag Model

A fundamental scenario would be a single fiber break with propagating debonds between the broken fiber and the two adjacent fibers (cf. Figure 1). The behavior of this elementary case, in a general sense, would reflect the behavior of a more complex damage state with multiple fiber breaks and growing debonds. Therefore, the case with a single fiber break with debonding will be subject to scrutiny to isolate the debonding process and the subsequent fiber rupture in a well-defined and simple configuration. A schematic picture is shown in Figure 6, and micrographs from experiments on the carbon fiber/epoxy composite are found in Figure 1. At the outset, there is a single fiber break at the origin in fiber number 0. The normalized length of the debonds in all four quadrants is α with the fiber break at the origin. Due to geometric symmetry, the analysis can be reduced to only one quadrant, i.e., a quarter-plane with the fiber break in the corner and a debond length α. The debonds are in matrix bays number

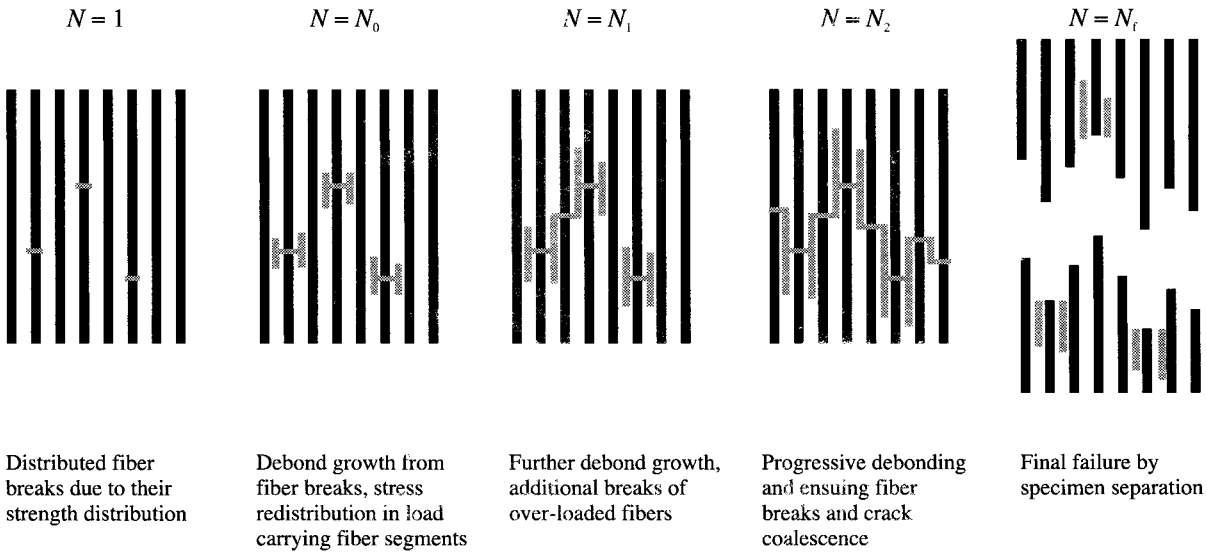

Figure 5 Schematic illustration of fatigue damage development and failure with increasing number of load cycles ($1 < N_0 < N_1 < N_2 < N_f$).

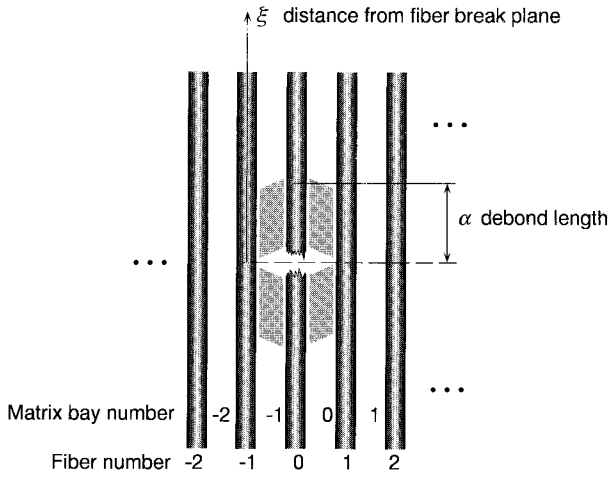

Figure 6 Single fiber break with debonds in an infinite two-dimensional composite.

0 and −1. The stress profile of the fibers adjacent to the broken fiber will be investigated in some more detail, since it is generally the next one to be broken. In order to calculate these stresses, a shear-lag model can be used. The two-dimensional shear-lag model developed by Beyerlein and Phoenix[8] was chosen to calculate the stress concentration profile in a fiber adjacent to a single fiber break. The main features of the model and the specifics of the present configuration are briefly outlined here. For details, the reader is referred to the cited original work.[8] As is typical for most shear-lag models, the fibers are supporting only axial loads, and the matrix transfers the loads in the fibers through shear only. The fibers are arranged equidistantly in an infinite two-dimensional array. Poisson contractions and stresses in the transverse direction are altogether neglected. One drawback is that the stress-concentration factors calculated by the Beyerlein–Phoenix model are independent of the volume fraction of fibers, but can still be used to analyze composite monolayers if the interfiber distance is held constant.[23]

Alternative models for monolayers have been developed by Ochiai et al.[24] and Wagner and Eitan.[11] The former model also accounts for tensile stress in the matrix, which can be useful for monolayer experiments with large interfiber distances. The latter model[11] accounts for the volume fraction of fiber by letting the "masked" part of intact fibers be approximately inactive to shear-stress transfer. The model[8] presently used is straightforward, compact, and based on physical reasoning. It is well suited for polymer-matrix composites, in particular for carbon fiber–reinforced plastics. Since the fiber-to-matrix stiffness ratio is very large, the constraints imposed by the shear-lag assumptions of tensile stresses in the fibers and shear stresses in the matrix do not impair the model. This is further emphasized by the high-volume fraction of fibers in commercial materials. However, in model specimens of composite monolayers, the stress concentration and fiber break evolution are known to depend on the interfiber distance,[25,26] and this dependency ought to be taken into account.

First, the constitutive relation can be expressed in dimensional units. The distance from the fiber break plane is x, the fiber spacing is w, and h is the ply thickness. The constitutive equation of the axial deformation of the fibers can be expressed as

$$p_n(x) = E_f A \frac{du_n(x)}{dx} \tag{1}$$

where $p_n(x)$ is the axial stress in fiber number n, E_f is the Young's modulus of the fibers, A is the cross-sectional area of a fiber, and $u_n(x)$ is the axial displacement in fiber number n. The constitutive law for matrix shear deformation is

$$\tau_n(x) = G_m \frac{u_{n+1}(x) - u_n(x)}{w} \tag{2}$$

where $\tau_n(x)$ is the shear-stress profile in matrix bay number n, and G_m is the matrix shear modulus. Combining the two constitutive laws with the condition of static equilibrium, the following differential equation presents itself:

$$E_f A \frac{d^2u_n(x)}{dx^2} = -\frac{G_m h}{w}[u_{n+1}(x) - 2u_n(x) + u_{n-1}(x)] \tag{3}$$

Second, a normalization would render this differential equation dimensionless, and the solution would be independent of the material properties and the composite geometric parameters. The fiber displacement is assigned to be

$$U_n(\xi) = \frac{u_n(x)}{p^* \sqrt{\frac{w}{E_f A G_m h}}} \tag{4}$$

where the dimensionless axial coordinate is

$$\xi = \frac{x}{\sqrt{\frac{E_f A w}{G_m h}}} \tag{5}$$

and the scaling factor is

$$p^* = \sigma^* \sqrt{\frac{w E_f A h}{G_m}} \tag{6}$$

where σ^* can be arbitrarily chosen to keep the order of magnitude of the stresses close to unity. The fiber stress becomes

$$P_n(\xi) = \frac{p_n(x)}{p^*} \tag{7}$$

and the matrix shear stress $T_n(\xi)$ and shear strain $\Gamma_n(\xi)$ become identical in the elastic regime,

$$T_n(\xi) = \Gamma_n(\xi) = U_{n+1}(\xi) - U_n(\xi) \tag{8}$$

To give an idea of the size scale, the value $\xi = 1$ in eq. (5) would correspond to

$$x = \frac{\pi d_f}{4V_f} \sqrt{\frac{2(1 + \nu_m)E_f}{E_m}} \tag{9}$$

where d_f is the fiber diameter, V_f is the volume fraction of fibers, and E_m and ν_m are the Young's modulus and Poisson ratio of the matrix, respectively. This assumes a monolayer of cylindrical fibers spaced by matrix elements with a thickness equal to the fiber diameter. Since the real composite is three-dimensional and the model is essentially two-dimensional, this relation qualitatively translates orders of magnitude and ranks rather than accurate values. However, $\xi = 1$ compares to $x \cong 50$ to 120 μm obtained from eq. (9) for standard values of the constituent elastic properties and volume fractions of conventional polymer matrix composites with long continuous carbon fibers (input data from ref. 27). For the present carbon fiber–reinforced epoxy, $\xi = 1$ corresponds to $x \cong 60$ μm.

The differential eq. (3) can be reexpressed in a nondimensional form as

$$\frac{d^2U_n(\xi)}{d\xi^2} + U_{n+1}(\xi) - 2U_n(\xi) + U_{n-1}(\xi) = 0 \tag{10}$$

from which solution the fiber stress can be calculated,

$$P_n(\xi) = \frac{dU_n(\xi)}{d\xi} \tag{11}$$

As outlined by Phoenix and coworkers, the determination of the stress state in the fibers can be reduced to the solution of two basic problems: the stress redistribution due to (1) an isolated fiber break and (2) an isolated shear-load couple. The numerical problem will be confined to a description of only the damaged regions (fiber break and debonds), from which the stress state in the entire volume can be formulated. In a finite-element approach, for example, the determination of the stress redistribution would demand a discretization and solution of the stress state in the entire volume. A finite element solution is also dependent on the choice of elements and mesh.

For the single fiber break at the origin, the boundary conditions are that $P_n(\pm\infty) = 1$ for the far-field applied load, and $P_0(0) = 0$ at the fiber break. Under these conditions, the break influence functions in the elastic case have been solved by Hedgepeth and Van Dyke.[28] They solved the isolated break problem analytically by a discrete Fourier transformation of eq. (10). The stress along fiber n_j at position ξ_j imposed by a unit compressive stress at the fiber break (which will later be compensated with a unit applied tensile stress) was determined to be

$$\Lambda = -\frac{1}{2}\int_0^\pi \sin\frac{\theta}{2} \exp\left(-2|\xi| \sin\frac{\theta}{2}\right) d\theta \tag{12}$$

Likewise, the shear stress and strain in matrix bay n_k at position ξ_k was shown to be

$$\Omega_k = \frac{\operatorname{sgn} \xi_k}{4}\int_0^\pi \left\{\cos(n_k + 1)\theta - \cos n_k\theta\right\} \times \exp\left(-2|\xi_k| \sin\frac{\theta}{2}\right) d\theta \tag{13}$$

where sgn($\cdot$) is the signum function, defined as +1 for a positive or zero argument, and −1 for a negative argument.

The influence of isolated shear couples has been deduced by Beyerlein and Phoenix,[8] who used a technique of quadratic influence superposition to ascribe inelastic properties from yielding and debonding to the matrix. In the present basic damage configuration, a simplified formulation with a set of shear couple point loads will be employed, but the deduction scheme from the aforementioned work will be used. In the shear-couple case, the boundary conditions of unit compressive load for the fiber-break case are exchanged by $P_n(\xi) = -\frac{1}{2}$ and $P_{n+1}(\xi) = \frac{1}{2}$, which correspond to a unit shear couple in matrix bay n at position ξ. The stress at the origin, i.e., the would-be position of the fiber break, due to an imposed shear load couple in matrix bay n_k at position ξ_k was determined to be

$$\Phi_k = \frac{\operatorname{sgn} \xi_k}{2\pi} \int_0^{\pi} \left\{ \cos n_k\theta - \cos(n_k + 1)\theta \right\} \times \exp\left(-2|\xi_k| \sin\frac{\theta}{2} \right) d\theta \quad (14)$$

Correspondingly, the shear stress/strain in matrix bay n_l at ξ_l caused by an applied unit shear couple in bay n_k at ξ_k became

$$\Psi_{lk} = -\frac{1}{\pi} \int_0^{\pi} \cos(n_l - n_k)\theta \sin\frac{\theta}{2} \times \exp\left(-2|\xi_k - \xi_l| \sin\frac{\theta}{2} \right) d\theta + \delta_{lk} \quad (15)$$

where δ_{lk} is Kronecker's delta function, which is defined as $\delta_{lk} = 1$ if $l = k$ and 0 otherwise.

The influence functions Φ and Ψ can be used to determine the local stresses in the composite imposed by debonds. In the debonded region, the stress-transfer ability of the matrix is reduced, and limited to frictional shear stresses. In fatigue, the debonded surfaces are continuously sliding against one another due to the repeated loading and unloading. The ensuing wear and attrition of the crack surface asperities are likely to make the frictional shear forces decrease continually during fatigue. Therefore, it is here assumed that there are no shear stresses in the debonded regions, $T = 0$. Since the measured fatigue debond lengths reported previously were large compared with the size scale of the microstructure (i.e., interfiber spacing), the effect from a yielded zone at the debond crack tip is neglected. Since the matrix material is constrained by stiffer surrounding fibers, the stress state in the matrix will be triaxial, which subdues large-scale yielding even for ductile polymers.[29]

Along the debonded strips in matrix bays -1 and 0 in Figure 6, a distribution of N shear couples are evenly dispersed to counteract the elastic response from other stress sources. To each shear couple k is a weight factor $K_{k,\mathrm{m}}$ allotted to account for its relative contribution. Similarly, the functions Λ and Ω are used to determine the local stresses contributed by the fiber break. The corresponding weight factor of the fiber break is denoted K_{f}. Combining the influences from both the fiber break and the debonded regions, the complete stress state in the composite can be established through the determination of the weight factors. These factors are determined from the boundary condition of a single fiber breaks with debonds without stress transfer:

$$\begin{pmatrix} K_{\mathrm{f}} \\ \mathbf{K}_{\mathrm{m}} \end{pmatrix} = \begin{pmatrix} \Lambda & \mathbf{\Phi} \\ \mathbf{\Omega} & \mathbf{\Psi} \end{pmatrix}^{-1} \begin{pmatrix} -1 \\ \mathbf{0} \end{pmatrix} \quad (16)$$

where -1 represents the unit compressive load at the fiber break, $\mathbf{0}$ is an N-dimensional vector assigning zero shear stress in the debonded regions. The elements Λ and K_{f} are scalars since only a single fiber break is considered. The submatrices $\mathbf{\Phi}$, $\mathbf{\Omega}$, and $\mathbf{\Psi}$ are of dimensions $1 \times N$, $N \times 1$, and $N \times N$, respectively. The weight factor vector $\mathbf{K}_{\mathrm{m}}$ is N-dimensional, the elements of which each pertain to an individual shear couple. Given the weight factors from the solution of eq. (16), the stress profile along any fiber can be calculated.

In like manner to the expressions of Λ and Ω in eqs. (12) and (13), the contribution from the fiber break and a matrix shear couple onto the stress profile in the adjacent fiber can be resolved. The adjacent fiber number 1 along the positive ξ-axis is selected, although the same stress profile is present in the other three quadrants due to symmetry. The stress profile in fiber 1 imposed by the fiber break is then expressed as

$$\lambda(\xi) = -\frac{1}{2} \int_0^{\pi} \cos\theta \sin\frac{\theta}{2} \exp\left(-2|\xi| \sin\frac{\theta}{2} \right) d\theta \quad (17)$$

and the stress profile in the same fiber imposed by a shear couple in matrix bay n_k at position ξ_k is by translation invariance expressed as

$$\omega_k(\xi) = -\frac{\operatorname{sgn}(\xi - \xi_k)}{2\pi} \int_0^{\pi} \left\{ \cos(n_k - 1)\theta - \cos n_k\theta \right\} \times \exp\left(-2|\xi - \xi_k| \sin\frac{\theta}{2} \right) d\theta \quad (18)$$

The stress profiles of the adjacent fibers are $P_1(|\xi|) = P_{-1}(|\xi|)$ due to symmetry. The stress profile in the selected quadrant is denoted $\Sigma(\xi) = P_1(\xi)$ for $\xi \geq 0$, which also corresponds to the stress concentration factor since the applied load is unity. With the stress factors K_f and $\mathbf{K}_m$ from eq. (16), the stress-concentration factor is

$$\Sigma(\xi) = 1 + K_f\lambda(\xi) + \sum_{k=1}^{N} K_{k,m}\omega_k(\xi) \quad (19)$$

where the first term 1 represents the influence from the applied load, which completely relieves the unit compressive stress at the fiber break.

Fiber Stress Profiles

The Matlab software package was used for the numerical calculations, where 10 to 20 shear couples were uniformly distributed along each of the four debonded lengths; $|\xi| \leq \alpha$, where the debond length α was varied between 0 and 2.25. In Figure 7, the stress-concentration factor in the neighboring fiber is plotted with respect to the distance to the fiber break plane for various debond lengths. Experimental investigations by means of micro-Raman spectroscopy support the calculated stress concentration in the adjacent fiber.[30–32] The elastic case with no debonding gives the highest stress concentration in the adjacent fiber with a value of $\Sigma = 1.3334$. The stress-concentration factors for full elastic and finite-element solutions in three dimensions is generically the same, but takes smaller maximum values than the preceding two-dimensional shear-lag solution, since more intact neighboring fibers can share the load released by the broken fiber.[33] It is doubtful if the elastic case with no debonds exists, since dynamic effects from sudden release of stored elastic energy when the fiber breaks should cause some additional damage besides the fiber break itself. The fatigue propagation of the debonds may therefore start at a some length larger than zero, $\alpha_0 > 0$. As the debond grows, the peak value decreases and moves away from the plane of the fiber break, and roughly follows the position of the debond crack tip. This behavior is in concert with other models and experimental measurements. The shapes of the stress profiles for different debond lengths are not unlike those obtained by Nedele and Wisnom[34] in an axisymemtric finite-element investigation. Lagoudas et al.[35] made a numerical investigation of the stress profiles near broken fibers using a shear-lag model with a viscoelastic creeping matrix, and obtained a broadening of the stress profiles as the viscoelastic relaxation of the matrix shear stresses progressed. Bennett and Young[36] have presented experimental data on moving peak axial fiber stresses with growing debonds by micro-Raman spectroscopy. With the same technique, Amer and Schadler[37] observed lower stress concentrations and wider distributions for a composite prone to debonding (fibers aged in boiling water) compared to a composite with relatively strong interface (pristine fibers). The peak value of the stress concentration factor in Figure 7 evens out, and seems result in a small overload, $\Sigma > 1$, which is presented in Figure 8.

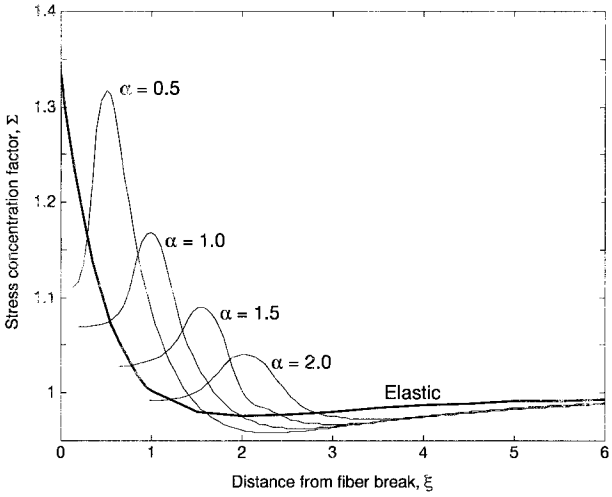

Figure 7 Stress concentration factor for different debond lengths.

The fiber break and its debonds give rise to a notably nonuniform stress profile along the adjacent fiber. As the debond propagates, the stress profile changes, which leads to relaxation of some of the previously overloaded parts of the fiber, whereas other parts close to the debond crack tip become more overloaded than heretofore. This continuous change in stress profile may eventually lead to rupture of the fiber at a point with an unprecedented overload. Increasing debond lengths will definitely result in an increasing probability of failure of a neighboring fiber.

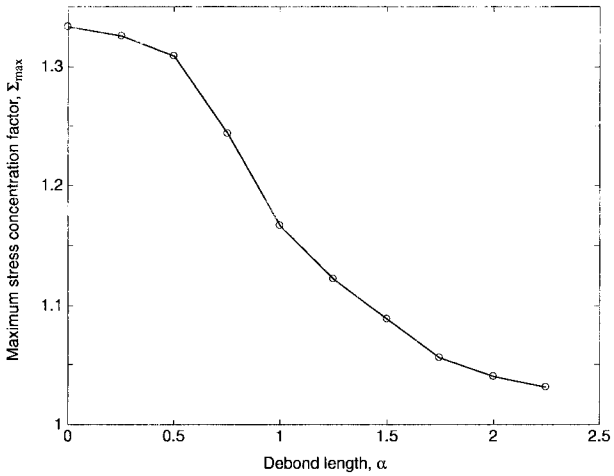

Figure 8 Maximum stress concentration factor as a function of debond length.

Probabilities of Fiber Failure

The statistical failure of a fiber adjacent to the broken and debonded fiber will be analyzed in particular. The fibers considered here are carbon fibers. They are known to have a strength that obeys reasonably well the Weibull distribution with the cumulative probability of failure

$$P_f(\Sigma_f) = 1 - \exp\left\{ -L\left(\frac{\Sigma_f}{\Sigma_0}\right)^{\beta}\right\} \tag{20}$$

where β is the shape parameter, Σ_0 is the scale parameter for unit fiber length (i.e., $L = 1$). The shape parameter can be interpreted physically as a measure of the flaw size distribution of the fiber.[38] It should be mentioned that linear scaling with L may not prove to be adequate for composite fibers over a large length range.[39,40] When the weakest link assumptions do not hold, the dependency on length in eq. (20) can be formulated as a power law with L^{γ} in lieu of L. A reason for this behavior can, for instance, be a variation in fiber cross-sectional area along its length. Typical values for the exponent γ are 0.6 for AS4 carbon fibers[41] and for aramid fibers,[42] and 0.9 for HS Celion 1000 carbon fibers,[40] and a range from 0.38 to 0.67 for various carbon fibers of Soviet origin.[39] Scaling with $\gamma = 1$ has been found to be quite appropriate with gage lengths within the same order of magnitude.[43] This linear behavior with $\gamma = 1$ as in eq. (20) will be used here.

The associated expectancy or mean value of the strength of a fiber segment with length L is

$$\bar{\Sigma}_f = \frac{\Sigma_0 \Gamma\left(1 + \frac{1}{\beta}\right)}{L^{1/\beta}} \tag{21}$$

where $\Gamma(\cdot)$ is the Gamma function.

In order to investigate the influence of scatter in fiber strength on the rupture of the fiber adjacent to the originally broken and debonded fiber, the mean strength $\bar{\Sigma}_f$ was kept constant for a number of different shape parameters β. The selected values are $\beta = 2$, 6, and 10, which represent experimentally obtained values for carbon and glass fibers.[27] By choosing the stress normalization parameter σ^* in eq. (6) so that $\Sigma_0 = 1$ for the middle value of the shape parameter $\beta = 6$, the mean strength is $\bar{\Sigma}_f = \Gamma(1 + \frac{1}{6})$ for unit gage length. The scale parameter for other shape parameters can then be calculated with

$$\Sigma_0(\beta) = \frac{\bar{\Sigma}_f}{\Gamma\left(1 + \frac{1}{\beta}\right)} \tag{22}$$

for $L = 1$. In this way, a parametric study of the influence of scatter in fiber strength on the breakage of the adjacent fiber can be undertaken without altering the mean fiber strength.

The investigated fiber segment can be partitioned into subsegments of length δ. The probability of survival of such a subsegment is

$$P_s(\delta, \Sigma) = \exp\left\{ -\delta\left[\frac{\Sigma}{\Sigma_0(\beta)}\right]^{\beta}\right\} \tag{23}$$

for a constant stress Σ. By use of the weakest link concept, the probability of failure of a fiber of length $\xi_0 = n\delta$ subjected to a nonuniform stress along its length can be estimated, if the fiber is divided into n pieces of length δ. The gage length is here chosen to be $\xi_0 = 6$, since the debonded stress profiles seem to be fairly close to the asymptotic value of the elastic stress profile at this point (cf. Figure 7). The probability of failure is

$$P_f(\Sigma(\alpha, \xi)) = 1 - \lim_{n\to\infty} \prod_{i=0}^{n} \exp\left\{ -\frac{\xi_0}{n} \times \left[\frac{\Sigma(\alpha, i\xi_0/n)}{\Sigma_0(\beta)}\right]^{\beta}\right\} \tag{24}$$

which yields

$$P_f(\Sigma(\alpha, \xi)) = 1 - \exp\left\{ - \int_0^{\xi_0} \left[\frac{\Sigma(\alpha, \xi)}{\Sigma_0(\beta)} \right]^\beta d\xi \right\} \quad (25)$$

where $\Sigma(\alpha, \xi)$ is the stress concentration at ξ in the fiber adjacent to the broken fiber for a unit applied load, and with a varying debond length α.

It should be noted that even if only the probability of failure of a gage length of one fiber ($0 \leq \xi \leq \xi_0$ in fiber number 1) is analyzed, the cumulative probability of failure in any of the four quadrants can be determined as

$$P_f^{tot}(\Sigma(\alpha,\xi)) = 1 - [1 - P_f(\Sigma(\alpha,\xi))]^4 \quad (26)$$

because of symmetry. For simplicity, we stick to only one fiber quadrant.

As the debond grows during fatigue, the stress profile along the considered fiber changes throughout the test. The fiber is subjected to a continuously changing nonmonotonic proof test. In an elastic material, it is the unprecedented stress at each given point that is critical, and that may cause failure. The envelope or maximum stress profile from the point where there was no debonding up to a debond length α is

$$\Sigma_e(\alpha, \xi) = \max_{0 \leq a \leq \alpha} \Sigma(a, \xi). \quad (27)$$

The probability of failure with respect to debond length is presented in a Weibull plot in Figure 9 for a unit applied load, and shape parameters $\beta = 2$, 6, and 10. The history and spatially dependent stress profile envelope Σ_e in eq. (27) was used to determine the probability of failure prior to a certain given debond extent. For all strength distributions, the probability of failure increases with increasing debond lengths. This is a necessary condition for a progressive-damage mechanism with successive fiber failures. Even though debonding is not a critical damage mechanism per se, it has an important influence on fiber breakage. Since the fibers constitute the main load-carrying members in polymer-matrix composites with continuous fibers, the failure of the composite can be caused only by failure of its fibers.

The probability of failure is significantly larger for higher values of β. With a narrower distribution of fiber strength, the composite shows higher sensitivity to local stress concentrations. The notch-insensitivity of composites with fibers with

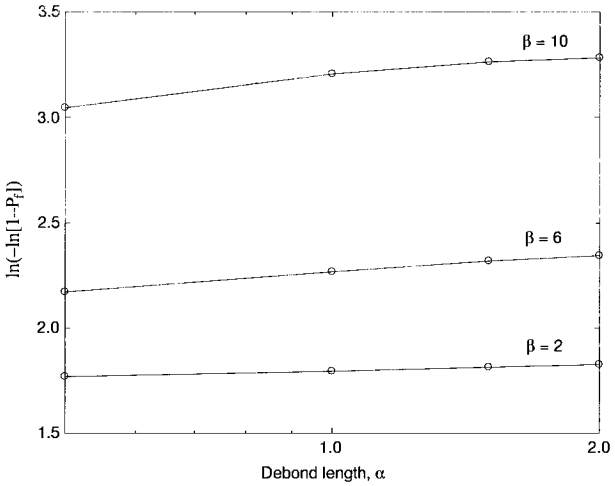

Figure 9 Weibull plot of the probability of fiber failure with respect to debond length and fiber strength variability.

a wide strength distribution has been investigated by Monte Carlo simulation by Beyerlein and Phoenix.[44] The simulations presumed length-invariant strength and no debonding. The flaw tolerance for small values of β was particularly large for small notches or cracks. Wagner et al.[45] studied fiber interactions in a composite monolayer with Kevlar fibers using micro-Raman spectroscopy, and found planar failure of fibers, despite a very small stress concentration from broken fibers. This can be explained by the relatively uniform strength of Kevlar fibers (small scatter compared with, e.g. carbon fibers). In contrast, fiber breaks are more spatially distributed in a composite monolayer with brittle carbon fibers possessing a considerably wider strength distribution, unless the fibers are brought to a close vicinity to one another so that strong interaction occurs.[26] A fiber type with a larger variability in strength provides a toughening effect due to its relative insensitivity to high overloads. This effect can be further enhanced by alteration of the path of progression of fiber fractures up to instability, as discussed later. This toughness can be interpreted as fracture energy, which is the sum of the energy consumed by all fiber breaks and the total amount of debond growth. Therefore, a composite with a wider distribution of fiber strength, hence more fiber breaks, and a propensity to debonding would render a material with a higher fracture energy. Such a material would be able to tolerate more damage, since it could accumulate more fiber breaks and debonds without failure of the composite.

As the debonds grow, and the stress profile in the neighboring fiber changes, so will the expectancy of the distance from the original fiber break to the secondary break $\bar{\xi}_f$. With no debond, the stress concentration is relatively localized to the plane of the original fiber break, but as the debond propagates, the stress-concentration profile becomes more distributed along the ξ-axis, and rupture is expected further away from the first break. With a narrow distribution of fiber strength, planar fiber breakage would be more likely. To investigate this supposition, a Monte Carlo simulation was undertaken. Through inversion of eq. (20), the strength of fiber segment i of length δ is

$$\Sigma_i = \Sigma_0(\beta)\left(-\frac{\ln Z_i}{\delta}\right)^{1/\beta} \tag{28}$$

where Z_i is a generated random variable from the uniform distribution between 0 and 1. Each of the 100 assigned fiber elements was then compared with the local stress, and the position of the weakest element with lowest positive strength to stress ratio was registered for 100,000 iterations for each stress profile and shape parameter. To isolate the effect of the damage inflicted stress concentration from the far-field applied stress, the local stress was somewhat unrigorously defined by subtraction of the applied stress from the present maximum stress profile, i.e., $\Sigma_e(\alpha, \xi) - 1$. In this manner, only fiber failures caused by the stress concentration from the present damage were generated. The mean value of the fiber break distance $\bar{\xi}_f$ was thus calculated for each debond length and fiber strength distribution. The simulation was repeated a number of times, and the maximum test-to-test difference was found to be no greater than 2%. The results of the simulations are presented in Figure 10. As the debonds grow, the mean distance to the second fiber break increases. With debonding, the overload on the adjacent fiber becomes more spatially distributed and fiber breaks tend to occur further away from the previous break. A more jagged and tortuous path between fiber breaks would then be expected for composites that are prone to debonding. In carbon fiber/epoxy, more planar fracture surfaces were observed in fatigue of composites with a strong interface.[46] This behavior also seems to hold for other kinds of unidirectional composite materials. Glass fiber–reinforced polypropylene with differing interfacial properties has shown a more straggling fracture appearance for the weaker interface after fatigue failure,[47] which can be explained by the abundant debonding that occurred in the weak interface material.[48] This pattern manifests itself even for certain metal-matrix composites. Naik et al.[49] observed distributed nonplanar fiber breaks for titanium matrix composites with weak interfaces, whereas those with stronger interfaces showed localized and planar fiber breakage. In short, a more uneven, broomlike failure mode of the composite specimens are prone to debonding, whereas composites with stronger interfaces, e.g. carbon fiber/epoxy, display a more planar fracture surface (see schematic picture in Figure 11).

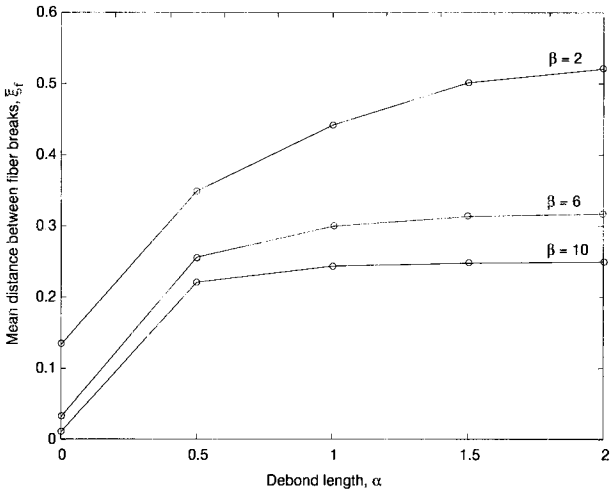

Figure 10 Mean distance to secondary fiber break with respect to debond length.

Figure 10 also shows that larger fiber strength variability, i.e., smaller values of β, leads to longer mean distance between fiber breaks. With a wider distribution in strength, the composite becomes less notch sensitive, i.e., less susceptible to failure at local stress concentrations. Scanning electron microscopy of fracture surfaces of unidirectional carbon fiber/epoxy laminates have indicated that scatter in fiber strength together with debond propagation are responsible for a more winding and distributed crack propagation.[50] In the extreme case where the fibers have a uniform constant strength ($\beta \to \infty$), the fibers will always fail in the same plane as the original fiber break, if it would fail at all, resulting in a planar fracture surface. The influence of growth of debonds would not result in any fatigue degradation, but only make already existing fiber breaks link up. In contrast, a large variability in fiber strength re-

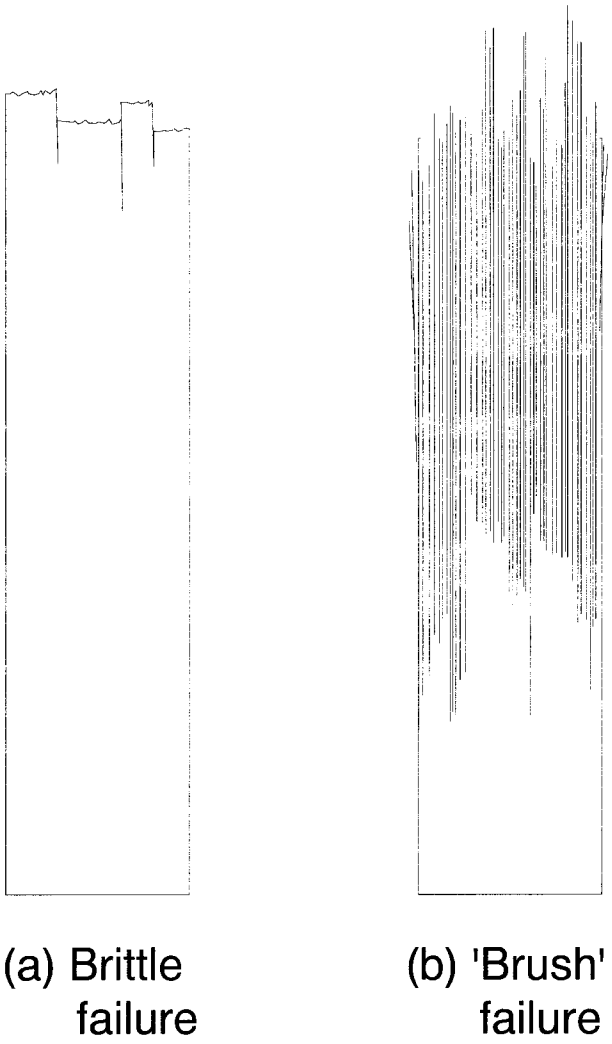

Figure 11 Fracture appearance: (a) brittle planar failure; (b) brushlike sprawling failure.

sults in longer average distances between fiber breaks, which means a more uneven and zigzagging linkup between breaks. This is the same feature that arises for debonding, and at low fatigue amplitudes. At high-cycle fatigue at low amplitudes, the debonds have time to grow to a considerable extent, which further affects fiber breakage. Schematic pictures of this relation are presented in Figure 12. How damage propagates from a notch or a flaw depends on the stochastic failure of fibers, which in turn depends on the nature of the stress distribution caused by growing debonds. Figure 12(a) illustrates distributed fiber breakage linked by propagating debonds. This scenario is prevalent for composites that are prone to debonding, have wide distributions in fiber strength, and are subjected to high-cycle

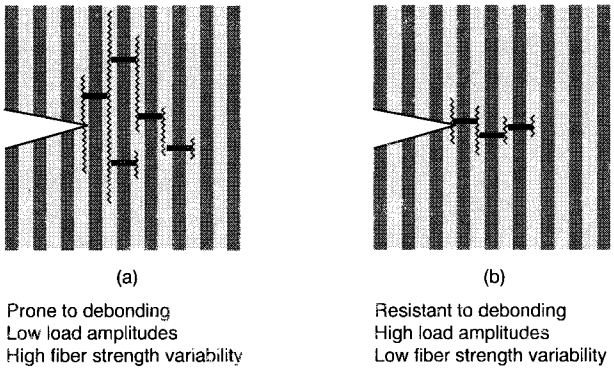

Figure 12 Illustration of damage development depending on scatter in fiber strength, debonding, and load level.

fatigue. The other scenario is the planar brittle type of fracture in Figure 12(b), which prevails in materials that are resistant to debond growth, especially for low-cycle fatigue. A low variability in fiber strength also favors this type of behavior.

The variability in the applied stress to cause failure in the adjacent fiber will vary depending on the stress profile and the distribution of fiber strength. A measure of the variability in applied stress that has resulted in fiber failure is the standard deviation, which is the square root of the variance, $s^2 = \langle \Sigma_f^2 \rangle - \langle \Sigma_f \rangle^2$. The standard deviation in fiber strength is given by

$$s = \frac{\sqrt{\Gamma\left(1 + \frac{2}{\beta}\right) - \Gamma^2\left(1 + \frac{1}{\beta}\right)}}{\left(\int_0^{\xi_0} \left[\frac{\Sigma_e(\alpha, \xi)}{\Sigma_0(\beta)}\right]^\beta d\xi\right)^{1/\beta}} \tag{29}$$

and is plotted in Figure 13. Naturally, the standard deviation of failure of the adjacent fiber is larger for fibers with larger scatter in strength, irrespective of the applied stress profile. More noteworthy is the trend that the variation in fiber strength decreases as the debonds grow. This is because $\Sigma_e(\alpha, \xi)$ becomes more distributed along ξ for larger α, which can be seen in Figure 7. The stress concentration becomes more evenly shared along the fiber, and thus turns the event of fiber failure less susceptible to local variations in fiber strength.

Returning to Figure 12(a), where the more widespread state of damage with ample stress soothing debonds result in a more homogeneous stress field, further damage propagation through

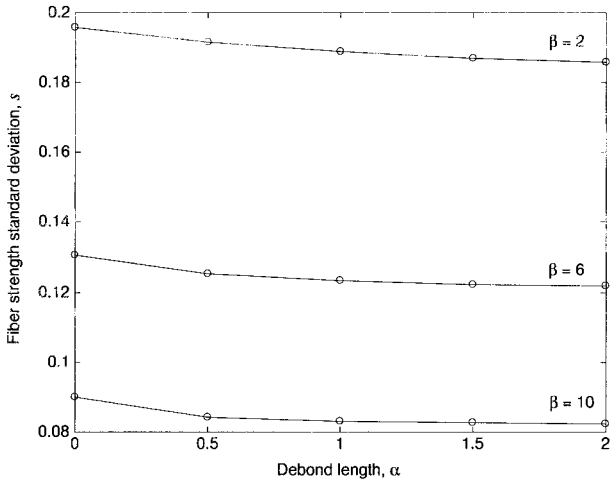

Figure 13 Standard deviation of strength with respect to debond length.

fiber breakage would be more predictable with less scatter. In Figure 12(b), the damage is more localized with higher local stress concentrations. This implies larger variations in further fiber breakage and crack propagation. This trend has been observed by Beyerlein and Phoenix[44] in simulation of fracture of a one-dimensional composite, where large notch lengths with more overstressed fibers resulted in a relatively lower scatter in composite strength. Fernando et al.[51] measured less scatter in fatigue life for carbon/aramid fiber composite hybrids than in the neat carbon fiber–reinforced plastic. The incorporation of the low modulus aramid fibers with high extensibility provides a mechanism of deflecting and arresting cracks, which leads to more damage-tolerant material able to accumulate more distributed fiber breaks,[52] and hence a more uniform and delocalized stress state. Moreover, carbon fiber/PEEK has shown less scatter in strength as well as in fatigue life than did carbon fiber/epoxy.[9] In carbon fiber/PEEK, the fiber breaks were distributed by abundant debonding, whereas the fiber breaks with substantially less debonds were highly localized for the carbon fiber/epoxy material. Kim and Hartness[53] have made corroboratory observations with more fiber breaks in carbon fiber/PEEK compared to carbon fiber/epoxy in fatigue. Also in fatigue of metal matrix composites, the crack paths from notches have been observed as schematically shown in Figure 12(b) for the as-received composite, and crack paths as in Figure 12(a) for the heat-treated composite with oxidized and degraded interface, which led to enhanced debonding.[20] This behavior has been further substantiated by numerical simulations, where high interfacial shear strength and small variability in fiber strength led to brittle fracture with localized planar damage.[54]

The distribution of damage by debonding makes the damage propagation more deterministic and reduces the scatter in strength and lifetime. An analogy can be made by considering a brittle ceramic where failure is controlled by the largest flaw, and therefore shows a large scatter in strength. In contrast to this, a ductile polymer material undergoes global yielding under deformation, and the yield stress shows very little variation from one test sample to another. Local load sharing or localization of damage, in general, leads to wide scatter in strength and fatigue life, but global load sharing or distributed damage accumulation results in a narrow scatter in strength and life.

In this context, a qualitative reasoning indicates that there is an optimum in static and fatigue properties with respect to interfacial debonding and scatter in fiber strength. First, with a high rate of debond propagation, the stress transfer between fibers becomes distributed along the load-carrying fibers. In the extreme case, the composite will act as a loose bundle with no stress transfer. Fatigue sensitivity is the disadvantage for rapid debond propagation. With no or little debonding, the composite is less sensitive to fatigue.[9,48] However, it is notch-sensitive with trade-offs in static strength due to its brittleness. Second, a wide distribution of fiber strength allows spatially distributed fiber breaks in the composite, which renders it more damage tolerant. However, the coalescence by debonding or yielding and subsequent failure are prominent in fatigue. The deterministic case with no distribution in fiber strength would result in planar crack growth as previously discussed. This has a deteriorating effect on the static properties, since stronger fiber segments may not be present at the crack tip to alter the crack path. Wagner and Steenbakkers[55] investigated damage propagation in composite monolayers and found aligned planar fiber breaks with aramid fibers that possess a relatively narrow distribution in strength, whereas the E-glass composite with its wide strength distribution showed multiply distributed fiber breaks. It should be appreciated that fiber breakage and debonding are mutually influencing mechanisms, and cannot be separated as their synergistic growth leads to final failure.

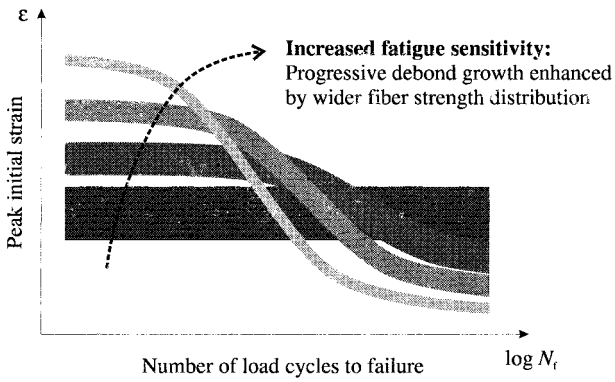

Figure 14 Influence of debond rate on fatigue sensitivity and scatter.

In the fatigue case, this synergism would lead to a more pronounced cycle dependency with increasing debond rates. The schematic illustration in Figure 14 portrays the influence of increased debond rate for a fix fiber strength distribution on the fatigue sensitivity and scatter in life. With increased debonding, the scatter would be mitigated because of more uniform and spatially distributed states of stress and damage. The progressiveness of debonding leads to a sloping fatigue life curve. This slope vanishes when debonding is fully suppressed, which is the case for some high modulus carbon fiber/epoxies, where the static strain to failure of the fibers is lower than the strain level of initiation of matrix or interfacial cracking.[10] Furthermore, the static strength is likely to be improved to some degree for moderate debonding since the debonds relax the stress concentration in the neighboring intact fibers and redistribute the load sharing to a larger volume of fibers.[56] For excessive debonding, the strength would decrease, and the composite would show bundle behavior and coalescence of fiber breaks. Only the case with a debonding that ranges from zero to moderate (for optimal static strength) is considered here. The fatigue limit would decrease somewhat since the limit load-carrying capacity decreases with increasing limit amount of debonds. This is true if there exists an arrest mechanism that stops further debond growth after a certain number of cycles (see, e.g., Figure 2). In the case of a fully debonded composite, the strain to failure is that of a corresponding loose fiber, which constitutes a lower bound in composites where global load-sharing conditions prevail.[57] These effects of debonding on fatigue life properties are further enhanced by a wider distribution of the fiber strength, since this would give rise to additional distributed breaks from which debonds can emanate.

APPROACHES TO FATIGUE LIFE PREDICTION

The lion's share of the fatigue life prediction schemes presented in the scientific literature concerns degradation of a macroscopic property, i.e., residual stiffness or strength, until final failure occurs. A fatigue-damage model based on the microscopic mechanisms would require less-costly testing, give better understanding, and provide indications for improvements of material properties. The models presented in this work are but a small step toward the ultimate goal of fatigue life prediction. It should be emphasized that a mechanism-based fatigue model demands extensive and precise experimental work to identify and quantify the operative fatigue-damage mechanisms, from which kinetic relationships intrinsic to the given composite material could be deduced. For life prediction, the kinetic equation must be complemented with a failure criterion. In the case of a shear-lag model, failure takes place when the fibers start breaking unstably.[44] This can be predicted directly by the model itself since the stress at all locations is given by the solution.

Micromechanical models for damage accumulation and life prediction in creep (sometimes termed "static fatigue") have been more frequently reported than micromechanical models for cyclic fatigue. Creep is also of great practical importance in durability of structural materials. Typically, a power law is applied to describe the viscoelastic constitutive equation of one of the constituents.[42,43] Creep is, like fatigue, a time-dependent process that results in irreversible damage or deformation, and may finally lead to failure. The mechanisms responsible for creep may very well be similar to those active in fatigue, although they propagate at different rates. Macroscopically, the applied load can be fluctuating (fatigue) or constant (creep), which microscopically gives rise to similar sets of basic damage mechanisms such as matrix yielding, debond growth, successive fiber breakage, etc. Creep models for life predictions have been developed for global load sharing,[57] in which distributed fiber breaks are unloaded equally by the all-surviving fiber in the same plane. Stress-life curves for creep in metal matrix composites have been successfully predicted with these models. Since

the rate of creep or debond growth in the matrix can be expressed arbitrarily, the models can be reformulated for a fatigue scenario. It is doubtful, though, if the approach of global load sharing can be used for polymer matrix composites, since the assumption of global load sharing is likely to be too crude.

In polymer matrix composites, the ratio between the maximum shear stress in the matrix to the characteristic fiber strength is relatively large, and local stress concentration close to fiber breaks will therefore be high compared to metal or ceramic matrix composites. A local load-sharing approach would therefore be more suitable for polymer matrix composites. Local load-sharing models for damage accumulation and life prediction become more detailed than those for global load sharing, since the individual damage sites have to be considered, as well as cluster formation and coalescence. A promising technique applicable to polymer matrix composites has been presented by Curtin and Takeda,[58] in which successive failures of interacting fiber segments with spatially dependent load transfer can be modeled in a three-dimensional lattice.

The present work has qualitatively highlighted relations between fiber breakage and debonding, and their influence on further damage growth in a fatigue framework. In a quantitative micromechanical model for fatigue life predictions of real polymer matrix composites, requisite features would be a three-dimensional description with local load sharing. The fiber strength distribution and the debond rate would be input parameters, both of which should be experimentally determined. Besides the potential to predict fatigue life at constant and variable amplitude loading, an accurate model would also allow for microstructural design for desired fatigue life and static properties.

CONCLUSIONS

There is ample experimental evidence that debonding is an active fatigue damage mechanism in unidirectional 0° carbon fiber–reinforced epoxy. It is subcritical in the sense that it does not directly result in final failure. Fibers must be broken to cause ultimate separation. However, the growing debonds redistribute the load in the neighboring fibers, and eventually a weak segment in one of these fibers may fail when it is overloaded. Subsequently, further debonding and fiber failures can ensue, until ultimate failure occurs. After experimental identification of these mechanisms by a surface replication technique, a parametric model was used to investigate debond propagation and its influence on stochastic fiber breakage. A shear lag model has been adapted for a single broken fiber with propagating debonds.[8] This constitutes a simple case to illustrate a fundamental type of damage propagation in fatigue of composite with weak interfaces. From damage influence functions, the stress in the fiber adjacent to the broken fiber was calculated with respect to the length of the debonds. A peak stress concentration factor propagates along with the debond at its tip, which results in a monotonically increasing probability of fiber failure. Also, debonding makes uneven and jagged crack propagation more likely, in which case the damage becomes more spatially distributed with a more homogeneous stress field. A large variability in fiber strength has basically the same break-distributing effect. With a more homogeneous stress distribution, the variability in strength decreases, which can explain the smaller scatter in fatigue life of composites that show a more homogeneous distribution of damage.

Part of this work was carried out at the Division of Polymer Engineering at Luleå University of Technology. Discussions with Dr. L. A. Berglund and financial support from the Swedish Research Council for Engineering Sciences (TFR) are gratefully acknowledged.

REFERENCES

1. Dauskardt, R. H.; Ritchie, R. O.; Cox, B. N. Adv Mater Processes 1993, 7, 26.
2. Dickson, R. F.; Fernando, G.; Adam, T.; Reiter, H.; Harris, B. J Mater Sci 1989, 24, 227.
3. Talreja, R. in Structure and Properties of Composites, Chou, T. W. Ed.; VCH: Weinheim, 1993; p 583.
4. Andersen, S. I.; Lilholt, H.; Lystrup, Å. in Design of Composite Structures Against Fatigue; Meyer, R. Ed.; Mechanical Engineering Publications: Bury St. Edmunds, 1996; p 15.
5. Hashin, Z.; Rotem, A. J Compos Mater 1973, 7, 448.
6. Awerbuch, J.; Hahn, T. in Fatigue in Composite Materials, STP 723; ASTM: Philadelphia, 1981; p 243.
7. Subramanian, S.; Reifsnider, K. L.; Stinchcomb, W. W. Int J Fatigue 1995, 17, 343.
8. Beyerlein, I. J.; Phoenix, S. L. J Mech Phys Solids 1996, 44, 1997.
9. Gamstedt, E. K.; Talreja, R. J Mater Sci 1999, 34, 2525.

10. Talreja, R. Proc R Soc London Ser A 1981, A378, 461.
11. Wagner, H. D.; Eitan, A. Compos Sci Technol 1993, 46, 353.
12. Ochiai, S.; Hojo, M.; Schulte, K.; Fiedler, B. Compos Sci Technol 1987, 57, 775.
13. Friedrich, K.; Walter, R.; Voss, H.; Karger–Kocsis, J. Composites 1986, 17, 205.
14. Xian, X. J.; Choy, C. L. Compos Sci Technol 1994, 52, 93.
15. Beyerlein, I. J.; Phoenix, S. L. Compos Sci Technol 1997, 57, 869.
16. Dharan, C. K. H. in Fatigue in Composite Materials; ASTM: Philadelphia, 1975; p 171.
17. Lorenzo, L.; Hahn, H. T. in Composite Materials: Fatigue and Fracture, STP 907; Hahn, H. T. Ed.; ASTM: Philadelphia, 1986; p 210.
18. Shih, G. C.; Ebert, L. J. Compos Sci Technol 1987, 28, 137.
19. Horstenmeyer, M. F.; Staab, G. H. J Reinf Plast Compos 1990, 9, 446.
20. Chan, K. S.; Davidson, D. L. Eng Fract Mech 1989, 33, 451.
21. Herring, H. W.; Lytzon, J. L.; Steele, J. H., Jr. Metall Trans 1973, 4, 807.
22. Jones, C. J.; Dickson, R. F.; Adam, T.; Reiter, H.; Harris, B. Proc R Soc London Ser A 1984, A396, 315.
23. Beyerlein, I. J.; Amer, M. S.; Schadler, L. S.; Phoenix, S. L. Sci Eng Compos Mater 1998, 7, 151.
24. Ochiai, S.; Schulte, K.; Peters, P. W. M. Compos Sci Technol 1991, 41, 237.
25. Chohan, V.; Galiotis, C. Composites Part A 1996, A27, 881.
26. van den Heuvel, P. W. J.; van der Bruggen, Y. J. W.; Peijs, T. Composites Part A 1996, A27, 855.
27. Hull, D.; Clyne, T. W. An Introduction to Composite Materials, 2nd ed.; Cambridge University Press: Cambridge, 1996.
28. Hedgepeth, J. M.; Van Dyke, P. J Compos Mater 1967, 1, 294.
29. Yee, A. F. in Toughened Composites, STP 937; Johnston, N. J. Ed.; ASTM: Philadelphia, 1987; p 383.
30. Schadler, L. S.; Amer, M. S.; Iskandarani, B. Mech Mater 1996, 23, 205.
31. van den Heuvel, P. W. J.; Peijs, T.; Young, R. J. Compos Sci Technol 1997, 57, 899.
32. Marston, C.; Gabbitas, B.; Adams, J.; Marshall, P.; Galiotis, C. Compos Sci Technol 1997, 57, 913.
33. Nedele, M. R.; Wisnom, M. R. Compos Sci Technol 1994, 51, 517.
34. Nedele, M. R.; Wisnom, M. R. Composites 1994, 25, 549.
35. Lagoudas, D. C.; Hui, C.-Y.; Phoenix, S. L. Int J Solids Struct 1989, 25, 45.
36. Bennett, J. A.; Young, R. J. Compos Sci Technol 1997, 57, 945.
37. Amer, M. S.; Schadler, L. S. Sci Eng Compos Mater 1998, 7, 115.
38. Jayatilaka, A. De S.; Trustrum, K. J Mater Sci 1977, 12, 1426.
39. Gutans, J.; Tamužs, V. Mech Compos Mater 1984, 20, 1107 (in Russian).
40. Watson, A. S.; Smith, R. L. J Mater Sci 1985, 20, 3260.
41. Beyerlein, I. J.; Phoenix, S. L. Compos Sci Technol 1996, 56, 75.
42. Phoenix, S. L.; Schwartz, P.; Robinson, H. H., IV. Compos Sci Technol 1988, 32, 81.
43. Otani, H.; Phoenix, S. L.; Petrina, P. J Mater Sci 1991, 26, 1955.
44. Beyerlein, I. J.; Phoenix, S. L. Eng Fract Mech 1997, 57, 241.
45. Wagner, H. D.; Amer, M. S.; Schadler, L. S. J Mater Sci 1996, 31, 1165.
46. Hahn, H. T. in Composite Materials: Testing and Design, STP 674; Tsai, S. W. Ed.; ASTM: Philadelphia, 1979; p 383.
47. van den Oever, M.; Peijs, T. Composites Part A 1998, A29, 227.
48. Gamstedt, E. K.; Berglund, L. A.; Peijs, T. Compos Sci Technol 1999, 59, 759.
49. Naik, R. A.; Pollock, W. D.; Johnson, W. S. J Mater Sci 1991, 26, 2913.
50. Theocaris, P. S.; Stassinakis, C. A. J Compos Mater 1981, 15, 133.
51. Fernando, G.; Dickson, R. F.; Adam, T.; Reiter, H.; Harris, B. J Mater Sci 1988, 23, 3732.
52. Peijs, A. A. J. M.; de Kok, J. M. M. Composites 1993, 24, 19.
53. Kim, R. Y.; Hartness, J. T. "The evaluation of fatigue behavior of polyether etherketone/graphite composite from prepreg tape," Reno (NV), April 3–5, 1984. in Proceedings of the 29th SAMPE Symposium, 1984; p 765.
54. Ochiai, S.; Sawada, T.; Hojo, M. Sci Eng Compos Mater 1997, 6, 63.
55. Wagner, H. D.; Steenbakkers, L. W. J Mater Sci 1989, 24, 3956.
56. Reifsnider, K. L. Polymer 1994, 35, 5035.
57. Fabeny, B.; Curtin, W. A. Acta Mater 1996, 9, 3439.
58. Curtin, W. A.; Takeda, N. J Compos Mater 1998, 32, 2042.